Chapter 4

Forest Health Assessment for Geo-Environmental Planning and Management in Hilltop Mining areas

This chapter has originally been published as: **Kayet, N**., Pathak, K., Chakrabarty, A., Singh, C. P., Chowdary, V. M., Kumar, S., & Sahoo, S. (**2019**). "Forest health assessment for geo-environmental planning and management in hilltop mining areas using Hyperion and Landsat data". **Ecological Indicators (Elsevier),** 106, 105471, SCI, Impact factor-4.95

4.1 Overview

Forest health assessment is a good concept in management of forest and natural resource. Mining activities in the iron ore belt of Saranda forest, Karo and Koina river basin which is a catchment area for these mines have a very high potential to induce forest health problems. Study area in the buffer zone of Kiriburu and Meghahatuburu mining fields are under high-stress conditions and are showing signs of dry and dying plant species. Growing mining related anthropogenic activities within and near the forest lands are causing threat to forest health. So it is essential to monitor forest health in surrounding mining sites.

4.2 Data acquisition and pre-processing

4.2.1 Data source

Hyperspectral (Hyperion) and multispectral (Landsat-OLI) data corresponding to the path and row number of 140/45 of Saranda forest, dated 16 Dec 2016 and 31 Dec 2016 respectively, were downloaded from the USGS website were used for this study. Forest health leaf spectra data were collected by field spectroradiometer instrument. GPS recorded healthy and unhealthy forest locations (latitude and longitude). Foliar dust data were collected in the field by PCE Instrument. NASA's EO-1 Hyperion satellite is equipped with Hyperion spectrometer that has the sampling spectral distance of 10nm within the 7.7 km swath path, which provides 242 spectral bands within the 350-2500nm wavelength of EM spectrum. Hyperion sensors provide images of surface features of the earth in hundreds of narrow adjoining spectral bands. Hyperion image was procured in georeferenced (1GST), radiometrically corrected (L1R), and terrain corrected (L1T) data format. Field Spectroradiometer based spectral data of healthy and unhealthy trees have been used for forest health classification and validation of results. GPS based healthy and unhealthy trees locations were used for forest health assessment. Field survey data obtained from the forest department of health and unhealthy tree locations were also used for forest health mapping. Toposheets and Google earth images were used for the justification of results.

4.2.2 Field spectra data collection

Field-based spectroradiometer recorded the healthy, moderately healthy, and unhealthy forest leaf reflectance spectra, and while collecting the reflectance spectra, canopy spectra were avoided. This instrument records the leaf reflectance spectra and their wavelength

within a range from 350 nm to 2500 nm. The field spectra containing 1024 bands at 1.4 nm (Visual), 2 nm (NIR), and 4 nm (SWIR) interval were then resampled to process 155 bands Hyperion data using the FWHM wavelength method. The field spectra were collected by SMA905 single fiber optic light guide having the FOV (Field of view) of 180°. The standard white reference panel had used for the measurement of white reference. A reflectance probe was used for measurements of leaf reflectance. The reflectance probe holder block was used for the sample distance (0-3/4″) and angle (45, 90, and 180 degrees) set. The forest pixels were masked, and the location of the sample was shown on the map (Figure 4.1).

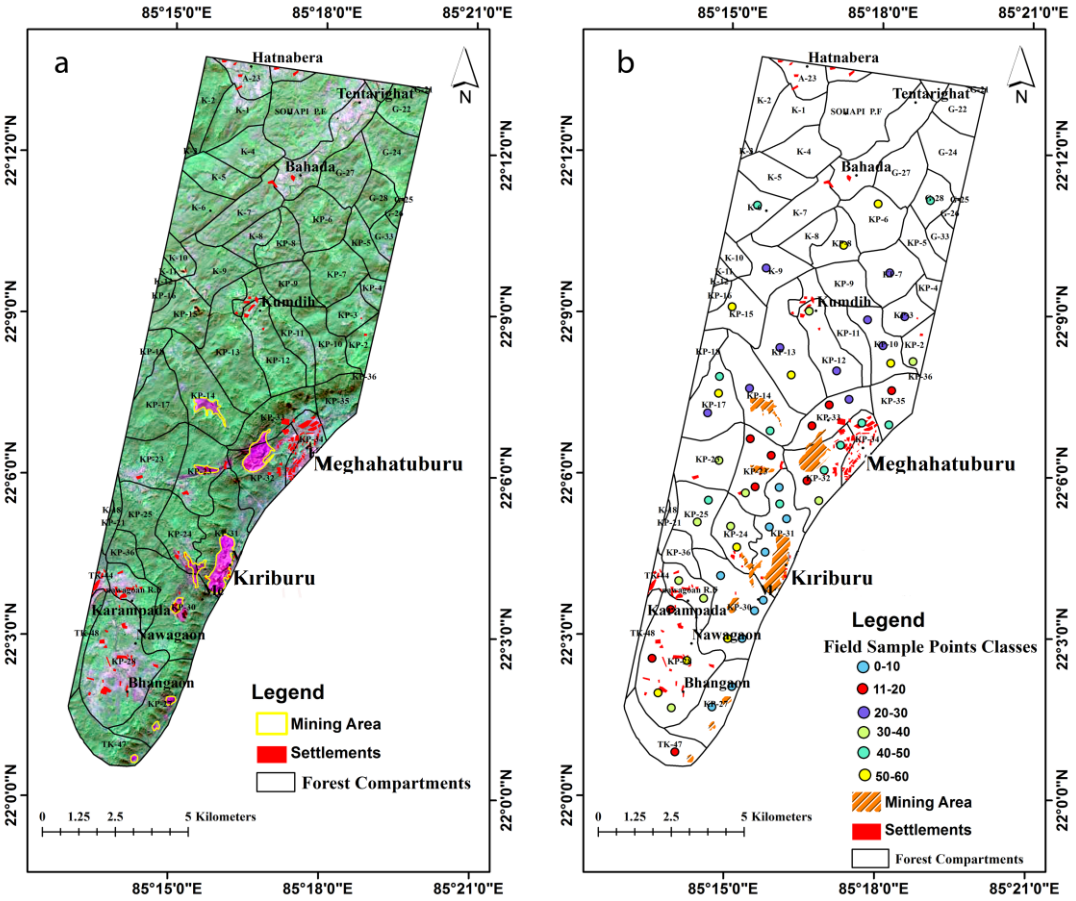

Figure 4.1: (a)Masking image used to eliminate forest pixels (left) , (b) Ground truth map indicating of collected filed samples (Right)

The field spectra for each forest health status were collected and mean spectra were used for the forest health assessment. GPS recorded the latitude and longitude of each sample location. Sixty sample points of forest health status were recorded by spectroradiometer in the field.

4.2.3 Lab spectral data collection

Leaves were collected from different tree species of the study area for lab spectra analysis. The leaves were plucked and enveloped in a plastic cover for lab spectra measurements that had to be made within 4 hours so as to maintain the leaves' optical properties (Vaiphasa et al. 2005). Measurement of leaves spectra of collected leaves; we had used a black room to avoid noise from other objects. The spectroradiometer and their lab accessories parts (pistol grip, reflectance probe, optic fiber cable, standard white reference panel, a halogen lamp, and sample holder) were used for laboratory leave spectra analysis. The pistol grip was attached to a fiber optic cable. The pistol grip was adjusted at an angle of 90°, and the sample holder was set at a distance of 2/3 inches from the leaf. The field of view of optic fiber cable was fixed at a 35° angle. The halogen lamp was selected having a wavelength, ranged between 350 to 2500nm as the energy source to create reflectance. A spectroradiometer recorded a total of 30 samples of lab spectra. The field survey and laboratory experiment to assess forest health was shown in Figure 4.2.

Figure 4.2: Spectroradiometry field survey (a) and laboratory analysis of collected spectra (b)

4.2.4 Pre-processing of field and lab collected spectra data

The field and lab collected spectra data were used to build a spectral library (Figure.4.3). We have developed a forest health based spectral library that could be used for forest health discrimination analysis and classification. The pre-processing of

lab and field spectra involved temperature drifts correction, water absorption correction, unilluminated wavelength removal, and spectral smoothing.

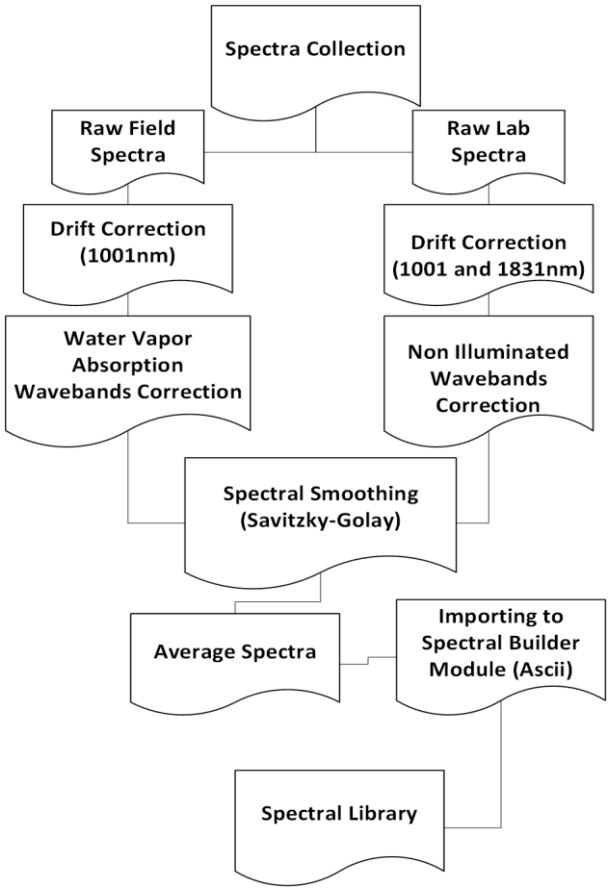

Figure 4.3: Pre-processing of raw spectra to build spectral library

The spectroradiometer is so structured that different inherent variations in detector sensitivity are used at different temperature conditions. Temperature drifts errors were generated due to multiple detectors used in the spectroradiometer. The spectra of different temperature drifts were located at 1001 nm and 1831 nm wavelength (Lenhard et al., 2005). The splice correction algorithm was used for spectral temperature drifts correction. During field spectra data collection, water-vapor errors come from ambient atmospheric components. The regions for water-vapor wavelength are generally located between 1350 to1460 nm; 1790 to 1960 nm, and 2350 to 2500 nm (Staenz et al., 2002). In lab spectra, the unilluminated error was coming from the halogen lamp. The regions of unilluminated error are generally located at 350 and 400 nm wavelength bands (Rogass et al., 2017). We have removed two types of error in wavelength bands (water vapor and unilluminated) from field and lab spectra. During spectral data collection, some noise was self-generated. Some researcher has used

linear and non-linear smoothing filters for spectral data smoothing. Savitzky-Golay algorithm based filter smoothing yields high accuracy (Vaiphasa, 2006; Savitzky & Golay 1964). So, we had used the Savitzky-Golay filter for spectral data smoothing. On spectral smoothing, the average spectra of tree health were calculated. The mean spectra (ASCII file format) were imported in spectral library builder options of ENVI. Then, we had built a spectral library of forest health with the help of other field surveys and secondary data.

4.2.5 Hyperion and Landsat-OLI data pre-processing

Hyperion (Hyperspectral) level 1 radiometric product is available in 242 bands. Hyperion radiometric image of which many of the bands are not working because of non calibrated, overlap region, water vapor absorption, and noise effected (Vyas et al., 2007). Finally, 155 Hyperion bands were considered for forest health analysis. The atmospheric correction has only reduced the effects of the atmospheric components, i.e., water vapor, dust, and gasses (George et al., 2014). The atmospheric correction was carried out by the FLAASH (Fast line of atmospheric sight analysis of spectral hypercube) model. Atmospheric corrected Hyperion data were further processed to remove shadow effect using a terrain correction model. Also, the Landsat-OLI (multispectral) data subjected to atmospheric correction and clouds and shadows were removed through a pre-processing image tool. Both Hyperion and Landsat -OLI data, were projected to Universal Transverse Mercator (UTM) coordinate system at WGS 84 datum, and zone 45° north. Atmospherically corrected data was used to MNF (Minimum Noise Fraction) transformation for noise removal. The MNF transformation is a linear transformation dataset, which is essentially a two cascaded PCA (Principal Components Analysis) transformations (Boardman and Kruse 1994). The PPI (Pixel Purity Index) algorithm was used, which is one of the widest end-member extraction algorithm used for Hyperspectral image analysis. PPI is a means of finding the most spectrally pure and extreme pixels in the Hyperspectral images (Vaiphasa et al., 2006). Hyperion image was added to the PPI algorithm for identifying spectrally pure pixels or end-members for selection of each forest health class. The spectral analysis tool was used for calculating the similarities measurement into field end-member average spectra, and Hyperion image derived average spectra. Two methods were used to measure the spectral similarity, i.e., SAM (Spectral Angle Mapper) and SFF (Spectral Feature Fitting).

4.3 Methodology

4.3.1 VIs model for forest health analysis

The narrow banded VIs (Vegetation Indices) model creates a spatial map that depicts the health and vigor of the forested region (Solberg et al., 2004). It well detects the healthy and unhealthy conditions of the forest. The VIs model uses four different narrow-bands vegetation indices. They are greenness VIs that shows the distribution of greenness; leaf pigment VIs which shows the concentration of anthocyanin pigments for stress levels; canopy water content VIs that shows the concentration of water; light use efficiency VIs that shows forest growth rate of the vegetation.

In the forest health assessment, vegetation indices are extracted from the Hyperion satellite image. Each of the vegetation properties is designed to represent some particular vegetation characteristics. Narrow-bands (Hyperspectral) VIs were also used for a forest health assessment (Table.4.1).

Table 4.1: Different narrow banded VIs for forest health assessment

Narrow banded VIs	Indices	Algorithm	Applications	References
Greenness Index	Modified Red Edge Normalized Difference Vegetation Index (MNDVI705)	$MRENDVI = \left(\frac{750nm \times 705nm}{(750nm+705nm(2*445nm))}\right)$	Precision agriculture, forest monitoring and vegetation stress detection.	Sims & Gamon,2002
	Modified Red Edge Simple Ratio (MSR700)	$MRESNDVI = \frac{\rho 750-\rho 445}{\rho 750+\rho 445}$	Precision agriculture, forest monitoring and vegetation stress detection.	Sims & Gamon,2002
	Red Edge normalized difference vegetation index (RENDVI)	$RENDVI = \frac{\rho 750-\rho 705}{\rho 750+\rho 705}$	Precision agriculture, forest monitoring and vegetation stress detection.	Sims & Gamon,2002
	Red Edge Position Index (REPI)	$REPI = \frac{p690-p740}{p700-p730}$	Sensitive to changes in chlorophyll concentration.	Curran., et al .1995
	Vogelmann Red Edge Index 1 (VREI1)	$VREI1 = \frac{p740}{p720}$	Vegetation phenology (growth) studies, Precision agricultural and vegetation productivity modeling.	Vogelmann,et al.1993

Canopy Water Content	Moisture Stress Index (MSI)	$MSI = \frac{\rho 1599}{\rho 819}$	Canopy stress analysis, Productivity and modeling fire hazard condition analysis.	Ceccato ,et al.2001
	Normalized Difference Infrared Index (NDII)	$NDLI = \frac{(P819-P1649)}{(P819+P1649)}$	Crop agricultural management, forest canopy mentoring and vegetation stress detection.	Jackson.et al.2004
	Normalized Difference Water Index (NDWI)	$NDWI = \frac{\rho 857-\rho 1241}{\rho 857+\rho 1241}$	Changes of canopy water content.	Gao,1995
	Water Band Index (WBI)	$WBI = \frac{\rho 900}{\rho 970}$	Changes of canopy water content.	Penuelas et al.,1995
Light Use Efficiency Index	Normalized Differences Lignin Index (NDLI)	$NDLI = \frac{\log(1/\rho 1754)-\log(1/\rho 1680)}{\log(1/\rho 1754)+\log(1/\rho 1680)}$	Estimate the amount of lignin in vegetation.	Serrano et al.,2002
	Photochemical Reflectance Index (PRI)	$PRI = \frac{\rho 531-\rho 570}{\rho 531+\rho 570}$	Estimation vegetation productivity and stress.	Gamon et al.,1992
	Red Green Ratio Index (RGRI)	$RGRI = \frac{\rho RED}{\rho GREEN}$	Estimate the course of foliage development in canopies.	Penuelas et al.,1995
	Structure Insensitive Pigment Index (SIPI)	$SIPI = \frac{\rho 800-\rho 445}{\rho 800-\rho 680}$	Effects of variation in canopy structure	Penuelas et al.,1995
Leaf Pigment Index	Anthocyanin Reflectance Index_1 (ARI-1)	$ARI\_1=\left(\frac{1}{\rho 550}\right)-\left(\frac{1}{\rho 700}\right)$	Sensitive to anthocyanin amount in vegetation.	Gitelson et al.,2001
	Carotenoids Reflectance Index_1 (CRI-1)	$CRI\_1=\left(\frac{1}{\rho 510}\right)-\left(\frac{1}{\rho 550}\right)$	Measure the amount of carotenoids in canopy.	Gitelson et al.,2002
	Carotenoids Reflectance Index_2 (CRI-2)	$CRI\_2=\left(\frac{1}{\rho 550}\right)-\left(\frac{1}{\rho 700}\right)$	Measure the higher Carotenoid concentrations	Gitelson et al.,2002

We had used the VIs model for four different ecological indices (Greenness, leaf pigments, canopy water content, and light use efficiency) in our study.

The coefficients of determination (R2) values for all narrow bands VIs were calculated. The Separability (S) Index between the two classes were calculated by the simple and robust method following Equation.4.1 (Landgrebe, 2003).

$$d_{norm}=\frac{(\mu_1-\mu_2)}{(\sigma_1+\sigma_2)} \qquad \text{(Eq-4.1)}$$

Where, μ and σ are the mean and SD (standard deviation) of the individual class respectively. We have collected 60 field samples and divided 6 classes based on dust

amount (g/m^2). Overall Separability (S) Index between different VIs class's combinations is calculated by following the Equation.4.2. (Landgrebe, 2003):

$$S=\frac{1}{15}\sum_{i=1}^{5}\sum_{j=i+1}^{6}\frac{|\mu_i-\mu_j|}{\sigma_i+\sigma_j} \qquad \text{(Eq-4.2)}$$

Where, i and j denote the vegetation indices classes. Our statistical pixel-based analysis for each VIs were calculated for test sample pixels and obtained the Pearson correlation coefficients (R^2) and Separability (S) value for different VIs sample pixels classes. In this work, the highest R^2 and S value of VIs were used for forest health model.

4.3.2 Forest health spectra assessment

The field-based spectroradiometer had collected the raw spectra in the study area (Figure.4.4). Hyperion end-member derived spectra were compared with the field spectra using spectral similarity score method (SSM), and the result is graded or weighted for each pair of spectra using spectral analysis tool (Somers and Asner et al., 2014).

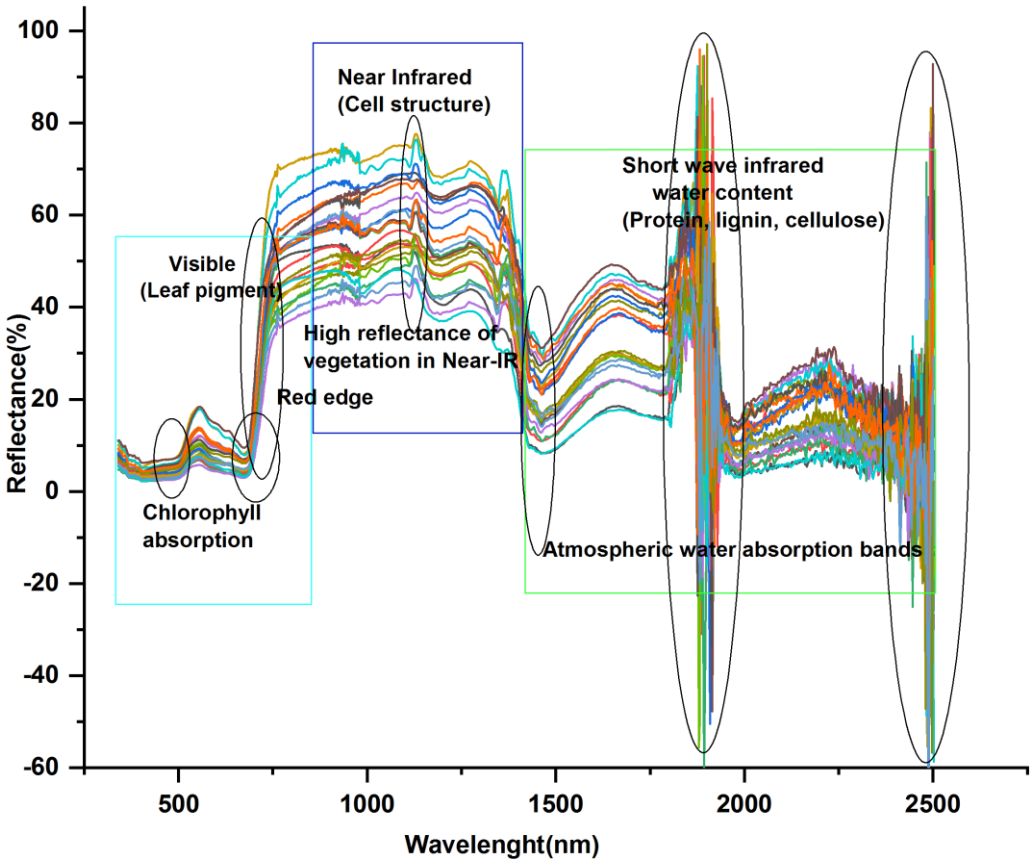

Figure 4.4: Raw field forest spectra obtained from field

The maximum value indicates the closest match and shows supper confidence in the spectral similarity. Spectral similarity output value below or equivalent to minimum show accurate matches and receives a score of 1. Zero scores are assigned for spectral similarity result greater than or equals to the maximum.

4.3.3 Classification techniques of forest health

Spectral Angle Mapper (SAM) is an algorithm, which is used for Hyperspectral image classification. SAM is a supervised image classification process. This method was used to calculate the spectral similarity between two spectra through deviation in radians angle between the satellite image spectra and reference spectra (Kruse et al., 1993). Spectral angle mapper identifies the spectral similarity using the following Equation.4.3 (De et al., 2002):

$$a=\cos^{-1}\left(\sum_{i=1}^{nb} t_i r_i \Big/ \left(\sqrt{\sum_{i=1}^{nb} ti^2}\right)^{1/2}\left(\sqrt{\sum_{i=1}^{nb} ri^2}\right)^{1/2}\right) \quad a=\cos^{-1}\left(\vec{\ } \vec{\ } \Big/ \| \ \| \right) \qquad \text{(Eq.- 4.3)}$$

Where α represents spectral angle between the vectors, nb denotes the number of spectral bands, t denotes target pixel, and r denotes reference pixel.

In this study, the SAM algorithm was used only for Hyperion image classification. For Spectral angle mapper based image classification on Hyperion data, the threshold value for various forest health classes was selected, ranged between 0.03o to 0.25o. The following threshold value of the highest radians angle viz., healthy (0.11), moderate (0.17), and unhealthy (0.20) were used for SAM classification. SAM classification parameters were used for higher accuracy measurement (Petropoulos et al., 2012).

SVM algorithm is the non-parametric supervised statistical-based image classification method. SVM classification generates highly accurate classification results than any other well-known ranking methodology such as a maximum likelihood or neural network classifier etc. (Bruzzone et al., 1995). The main objective of the SVM algorithm is to search for the Optimal Separating Hyperplane (OSH). The Proper

result from complex and noisy data can be derived from the SVM classification. OSH can be calculated by following the below-mentioned Equation.4.4:

$$\text{Minimize} \left\{ \frac{1}{2}\omega^2 + c \sum_{i=1}^{l} \xi_i \right\}$$

$$y_i \left[\omega^T x_i + b \right] \geq 1 - \xi_i, \qquad \text{(Eq-4.4)}$$

$$\xi_i \geq 0,$$

$$\text{Subject to}$$

$$i = 1, 2, ..., l,$$

Where, x_i indicates training vectors in a data-set $\{(x_i, y_i)\}_{i=1}^{l}$, and y_i is the associated label, ω indicates the weight vector, b indicates the bias, C indicates the penalty for misclassification, ξ_i indicates slack variables with non-negative constraint and allow misclassification of noisy data. The quadratic optimization problem is resolved and re-written as follows Equation.4.5:

$$f(x) = sign\left[\sum_{i=1}^{l} a_i y_i k(x, x_i) + b \right] \qquad \text{(Eq-4.5)}$$

Where a_i indicates Lagrange multipliers, $k(x, x_i)$ indicates the kernel purpose that projects the main training data into a higher-dimensional feature while computing non-linear decision surface.

In this study, the SVM algorithm was used for Hyperion and Landsat- OLI data for full pixel classification. For SVM algorithm, the radial function kernel category was selected having gamma value fixed to 0.31 for Hyperion and 0.137 for Landsat-OLI data (Tso et al., 2009). The SVM algorithm function with penalty parameter hundred and pyramid value zero was used for Hyperion and Landsat- OLI data classification. The SVM algorithm determines the optimal gamma and penalty values, generally uses grid exploration method.

4.3.4 Classification accuracy assessment

Accuracy assessment is an important work in the classification validation system. Remote Sensing technology is a great source of thematic map presentation systems, although accuracy assessment assists how far the classification represents the real

world (Congalton, 1991). The overall accuracy of the classified class's pixels was matched to reference ground data by the Equation.4.6 (Congalton, 1991).The SAM, SVM algorithms, and VIs model-based classified images were calculated for overall accuracy, and kappa statistic using field surveys reference data.

$$K = \frac{N\sum_{i=1}^{k} xii - \sum_{i=1}^{k}(x_{i+} \times x_{+i})}{N^2 - \sum_{i=1}^{k}(x_{i+} \times x_{+i})} \quad \text{(Eq-4.6)}$$

Where r indicates the number of rows in the error matrix, xii indicates the number of observations in the ith column, and row xi+ indicates the total number of observations in the ith column. N is the total number of observations. The overall research flow chart has been shown in Figure.4.5.

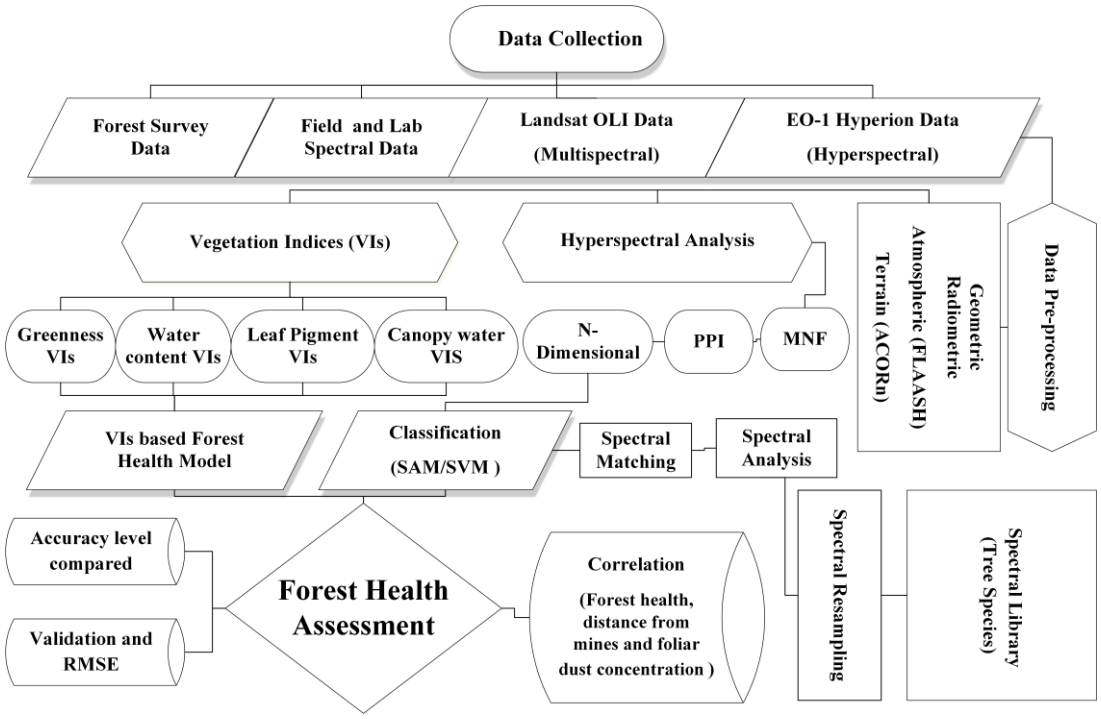

Figure.4.5: Research methodology for forest health assessment

4.4 Results and Discussion

4.4.1 Health and unhealthy pixels detection based on VIs model

The R^2 and S values for the VIs are shown in Table.4.2. When R^2 and S, acquired common values for MSR700, MSI, NDNI, and ARI1, VIs were comparatively high. Forest health mapping was accomplished by the use of narrow-band VIs viz.,

MSR700, MSI, NDNI, and ARI1. Each VIs class has upper and lower quartiles value as well as mean and median, the value of which is shown in Figure.4.6.

Table 4.2: Coefficients of determination (R^2) and Separability (S) values of forest health based on VIs model

Narrow banded VIs	Indices	Mean	SD	R^2	S
Greenness Index	MNDVI705	0.47	0.20	0.88	0.43
	MSR700	4.76	1.83	0.76	0.30
	RENDVI	0.52	0.21	0.79	0.28
	REP	0.71	0.01	0.04	0.16
	VOG1	1.67	0.40	0.48	0.01
Canopy Water Content	MSI	0.77	0.28	0.72	0.37
	NDII	0.51	0.15	0.58	0.07
	NDWI	0.54	0.16	0.42	0.21
	WBI	0.97	0.11	0.24	0.17
Light Use Efficiency Index	NDNI	0.08	0.02	0.59	0.29
	PRI	0.42	0.09	0.37	0.14
	RGR Ratio	1.17	0.28	0.49	0.15
	SIPI	1.01	0.25	0.50	0.12
Leaf Pigment Index	ARI1	9.15	3.05	0.66	0.32
	CRI1	11.90	2.68	0.45	0.24
	CRI2	13.85	1.65	0.23	0.21

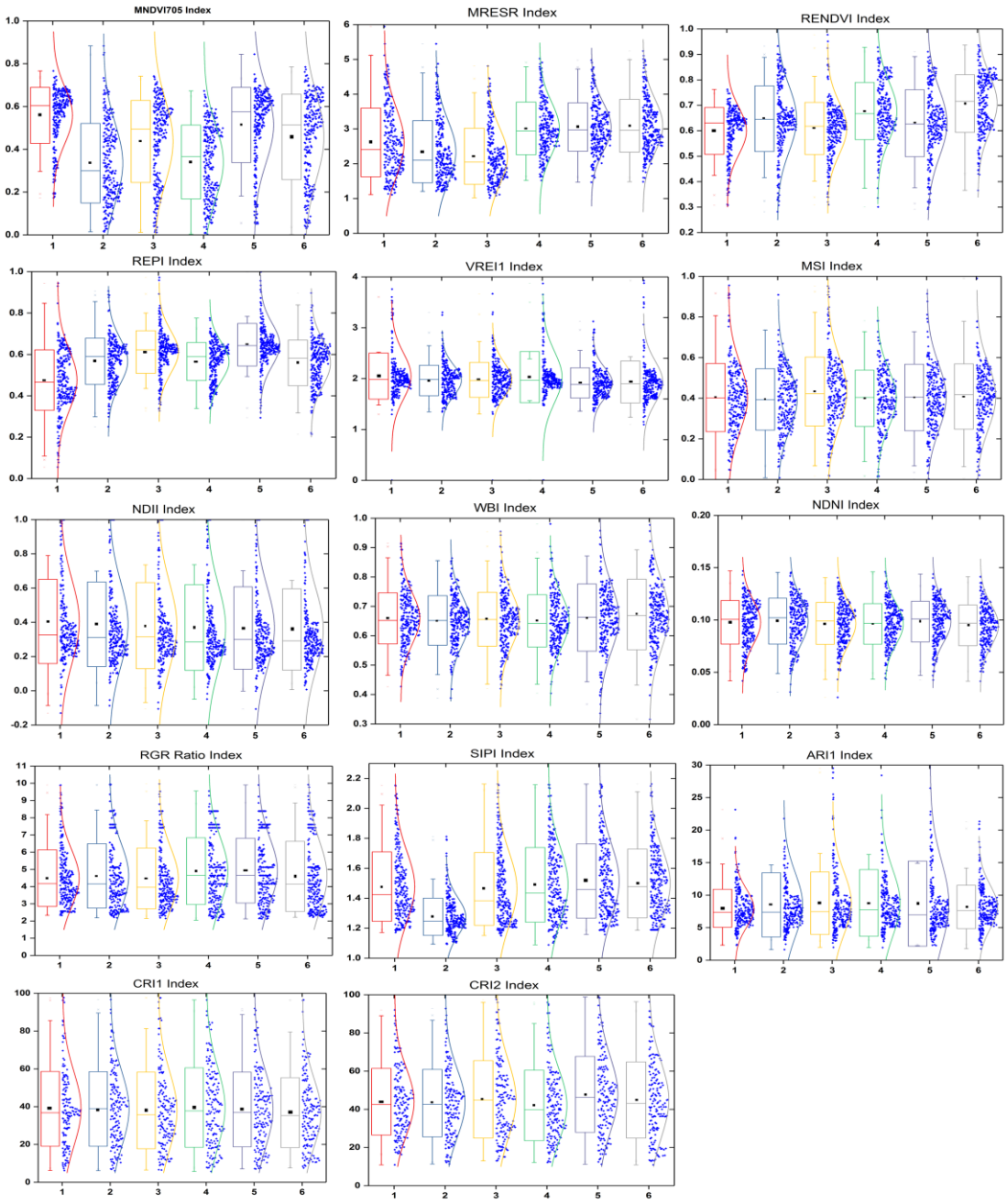

Figure 4.6: Mean, median, upper and lower quartile values of narrow banded VIs classes

The MNDVI705 is used for little changes in canopy foliage content, gap friction, and canopy subsequence. NDNI and MSI are sensitive to canopy carotenoid pigment in the plant leaf. ARI1 index is useful where there is a high variability is in canopy structure or leaf pigment index. VIs model based forest health map has classified the health into nine classes (Figure.4.7). Forest health class 1 represents unhealthy class, whereas class 9 represents a healthy class.

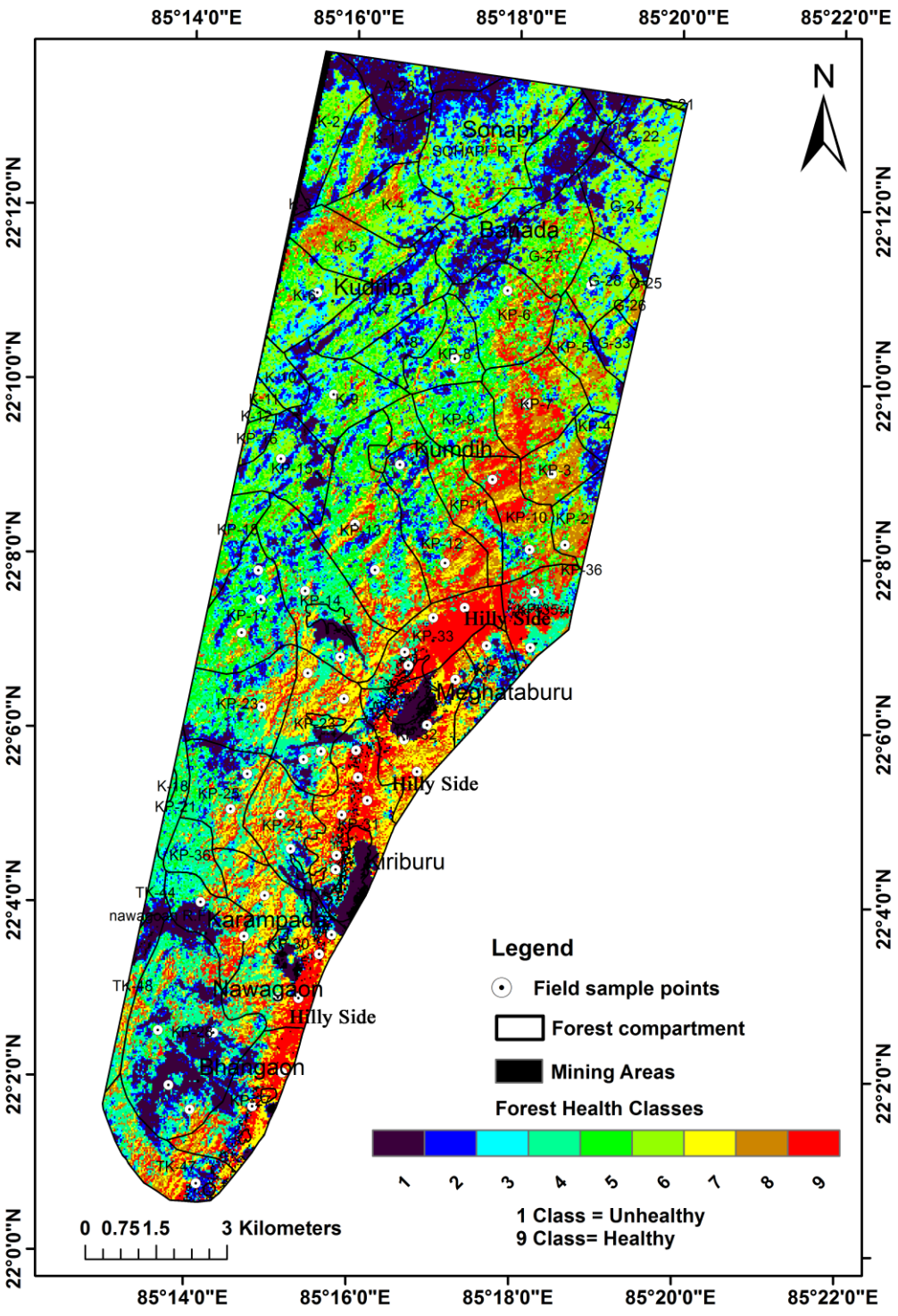

Figure 4.7: VIs model based forest health classes

4.4.2 Forest health spectra assessment

The spectral similarity score (SAM score) between two situ reflectance field-lab spectra and end-member spectra were educed from Hyperion image. The similarity scores shows that healthy forest (0.82), moderately healthy forest (0.79) and unhealthy

forest (0.67). As reported by the spectral similarity scores, the healthy forest has high similarity between two reflectance spectra. The SAM score for the moderate healthy forest was medium. The score of the unhealthy forest was found lowest. The average reflectance spectrum of different forest health has a variation for those collected from field (Figure.4.8).

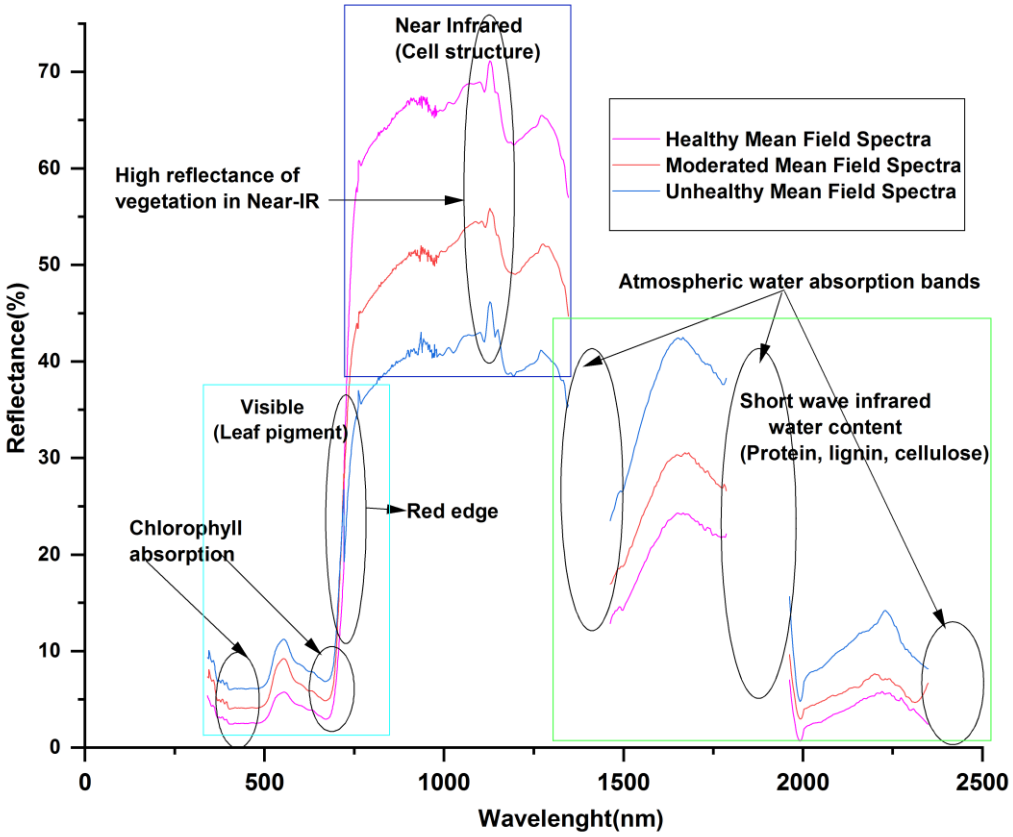

Figure 4.8: Visual comparison of resampled field average reflectance spectra of different forest health class.

4.4.3 Forest health classification and accuracy assessment

Figure.4.9 shows the VIs model, support vector machines and spectral angle mapper algorithms based on the forest health classification of images of Hyperion and also, SVM classified image of Landsat-OLI. In total, three forest health class (viz., healthy, moderate and unhealthy) were mapped in the study area.

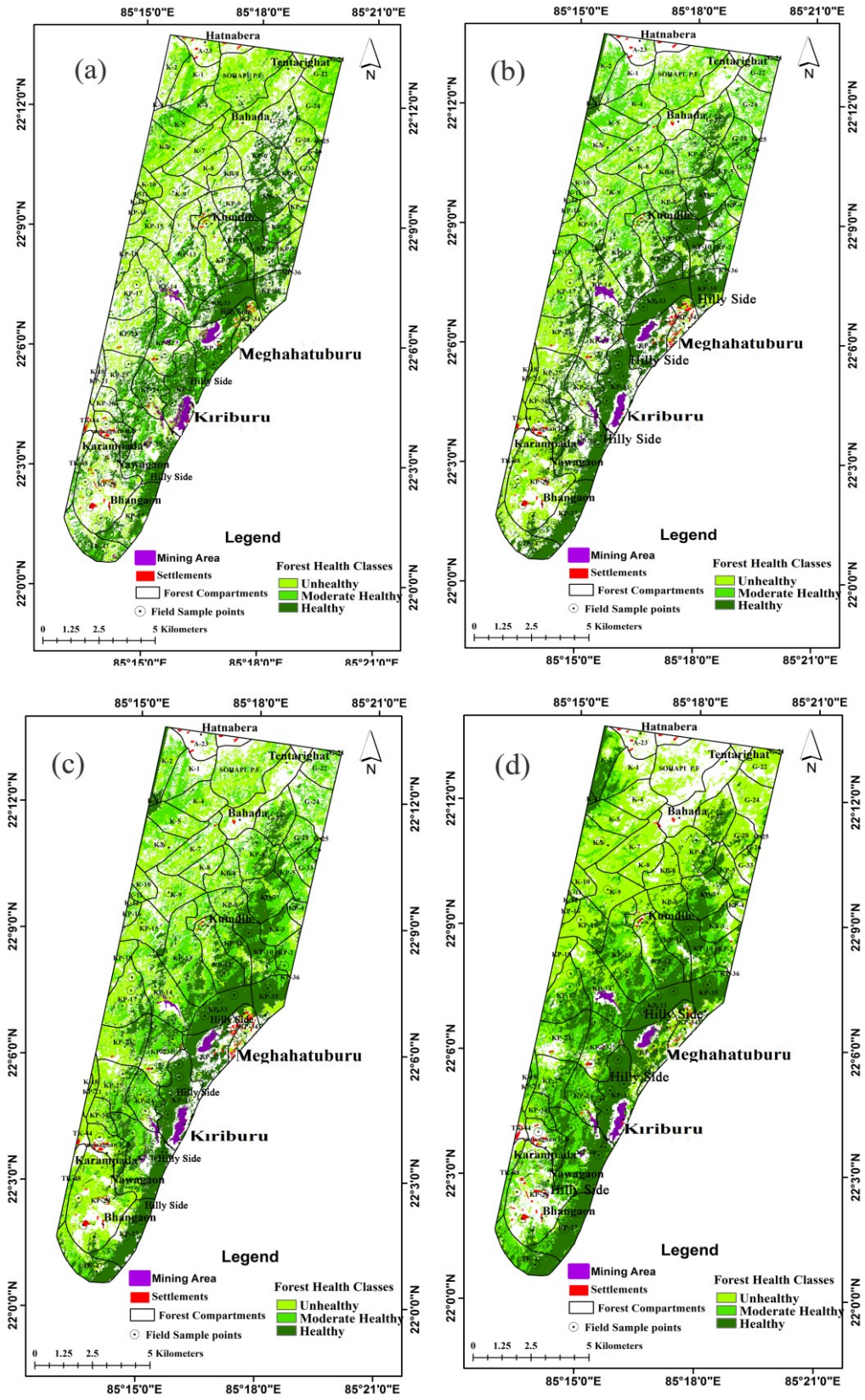

Figure 4.9: Forest heath mapping (a) VIs model based Hyperion (b) SAM based Hyperion (c) SVM based Hyperion (d) SVM based Landsat OLI

Healthy forest classes were distributed in the upper and lower part of Kiriburu and Megataburu mines as well as north-east and south-west part of the hilly sides .Moderately healthy forest covered the little portion of the study area and the rest area are covered by the unhealthy forest. The unhealthy forest is distributed mainly around the Kiriburu and Megataburu mine buffer area, agricultural area, scarps area, city, and fallow land area. The classification error matrices are shown in Table.4.3.

Table 4.3: Accuracy assessment results (a) SAM based on Hyperion (b) SVM based on Hyperion, (c) VIs based on Hyperion, and (d) SVM based on Landsat OLI

(a) SAM based on Hyperion	Healthy	Moderated Healthy	Unhealthy	Total	UA
Healthy	11	0	2	13	82.28
Moderated Healthy	0	11	1	12	75.51
Unhealthy	0	1	9	10	85.26
Total	11	12	12	35	
PA	90.49	83.53	66.33		
Overall accuracy: 79.55%, kappa statistics: 0.75					
(b) SVM based on Hyperion	Healthy	Moderated Healthy	Unhealthy	Total	UA
Healthy	11	0	1	11	81.52
Moderated Healthy	0	13	0	13	74.54
Unhealthy	2	0	10	12	70.66
Total	13	13	11	36	
PA	91.83	85.53	80.11		
Overall accuracy: 76.53%, kappa statistics: 0.71					
(c) VIs based on Hyperion	Healthy	Moderated Healthy	Unhealthy	Total	UA
Healthy	13	0	1	14	85.24
Moderated Healthy	1	11	0	12	78.95
Unhealthy	0	1	10	11	72.83
Total	14	12	11	37	
PA	90.84	81.76	76.52		
Overall Accuracy: 81.52%, Kappa Statistics: 0.79					
(d) SVM based on Landsat OLI	Healthy	Moderated Healthy	Unhealthy	Total	UA
Healthy	11	0	1	12	72.96
Moderated Healthy	0	9	0	9	64.54
Unhealthy	0	2	8	10	62.27
Total	11	11	9	31	
PA	72.96	64.54	62.27		
Overall Accuracy 67.21%, Kappa Statistics: 0.62					

4.4.4 Relationship among distance from mines, forest health and foliar dust concentration

Forest health conditions and nearby environments depend on its vicinity from the mines. The distance of sample points of forest health from mines were calculated. The foliar dust concentrations were collected from the field using the PCE instrument (Appendix.1). We have used Pearson correlation test methods for the study of the relationship between forest health classes, its distance from mines, and foliar dust amount (Table 4.4) for Kiriburu and Meghataburu mines.

Table 4.4: Pearson method based correlation matrix amongst forest health classes, foliar dust concentration and mine (Kiriburu) distance.

Pearson correlation	Forest Health classes	Leaf Dust Value (gm/m^2)	Distance(m) from Meghahatuburu Mine
Forest Health class	1	-0.67	0.22
Leaf Dust Value (gm/m^2)	-0.67	1	-0.45
Distance(m) from Meghahatuburu Mine	0.22	-0.45	1
Forest Health classes	1	-0.67	0.54
Foliar dust amount (gm/m^2)	-0.67	1	-0.48
Distance (m) from Kiriburu Mine	0.54	-0.48	1

We have tested the same relationship with another mine (Meghataburu), and it was found that the results are the same as those obtained for Kiriburu mine. Results obtained from the field survey show that there is a clear relationship between the distance from mines, forest health classes, and foliar dust concentration (Figure.4.10).

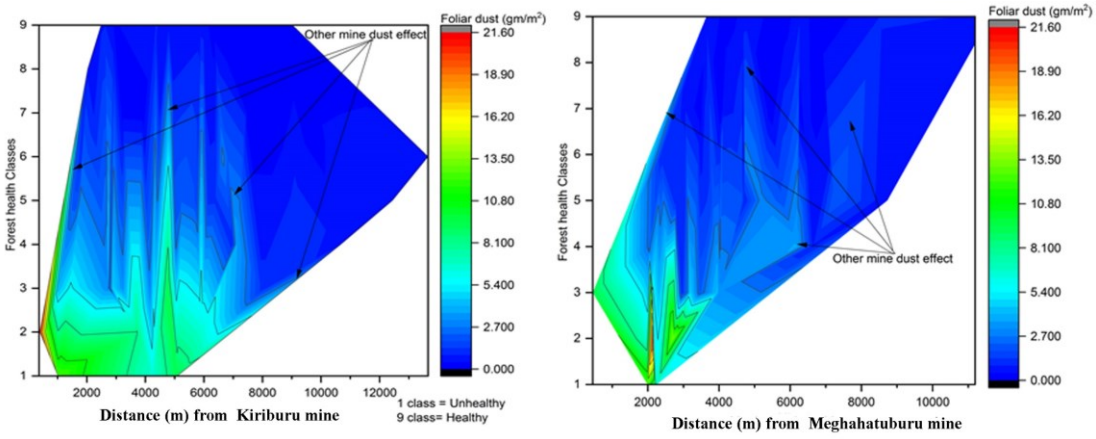

Figure 4.10: The relation amongst different forest health classes, distance from mines and foliar dust concentration (Kiruburu and Meghataburu)

4.4.5 Forest health validation

The healthy, moderately healthy, and unhealthy components constituting the forest of the study area were evaluated, both at ground level and pixel- level, having the highest reflectance data from the NIR wavebands region. The correlation determination (R^2) and RMS error values were evaluated from ground level and pixel-level spectral data (Figure.4.11). A correlation (R^2=0.84) was observed between the ground level and pixel-level for class healthy, and an RMS error of 3.98 was found. A correlation (R^2=0.86) was observed between the ground level and pixel-level for class moderately healthy, and an RMS error of 2.06 was found. And a correlation (R^2=0.87) was observed between the ground level and pixel-level for class unhealthy, and an RMS error of 1.25 was found.

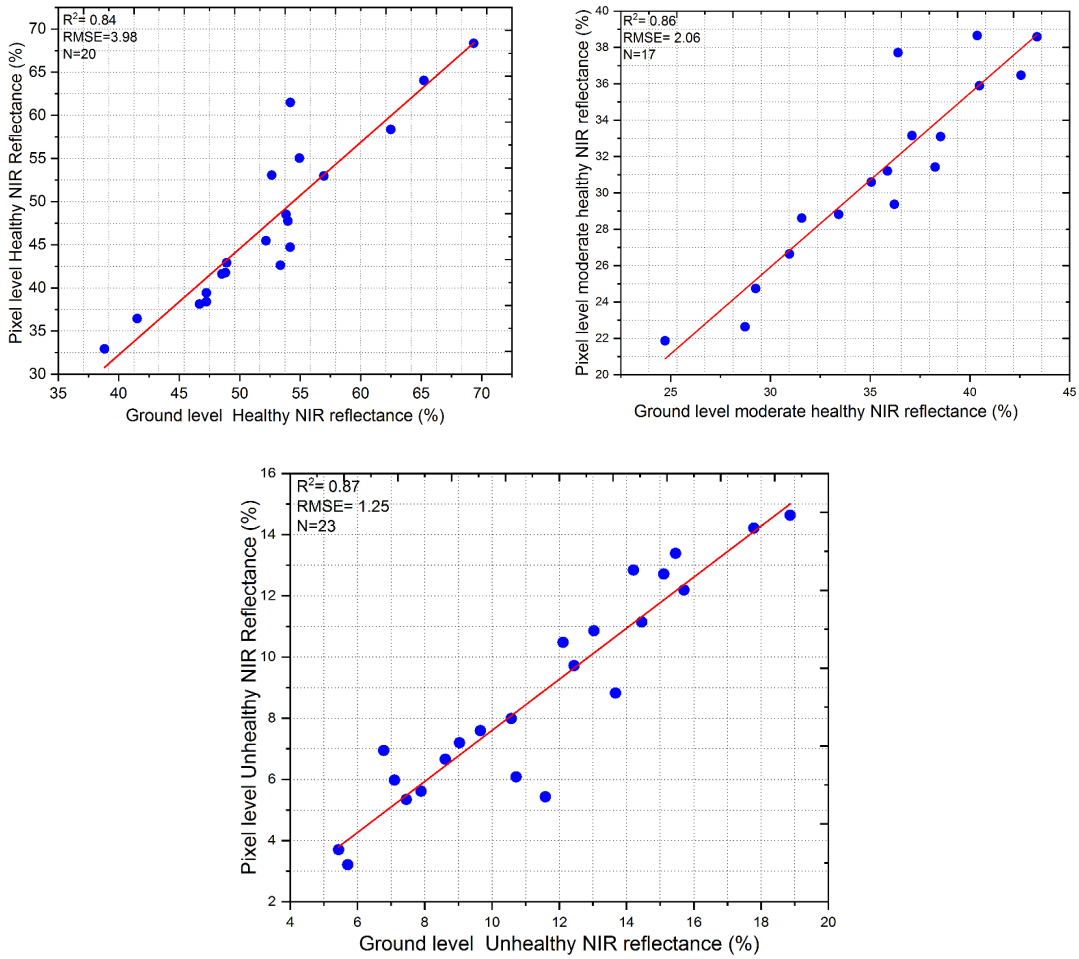

Figure 4.11: Correlation between field reflected spectra and pixel reflected spectra of healthy, moderate healthy and unhealthy forest class.

The six variables (ground level and pixel level: healthy, moderately healthy, and unhealthy) were presented in a scatter matrix (pair-wise scatter plot) plot (Figure.

4.12). It shows positive and negative correlation as well as standard error of six variables.

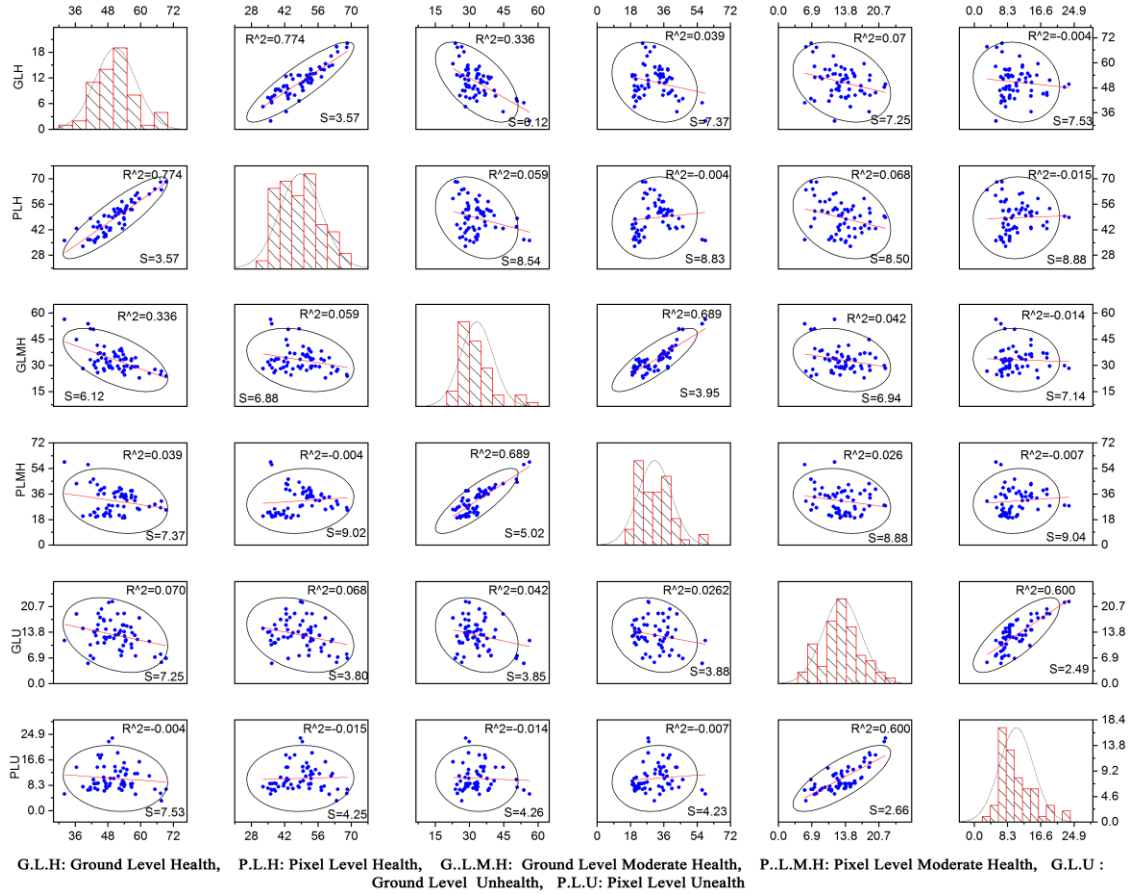

Figure 4.12: 6×6 Scatter matrix plot (3 from satellite data and 3 obtained from field data)

4.4.6 Discussion

As per the result obtained in this chapter, we could infer that, Hyperspectral data (Hyperion) has more capability in forest health assessment when coupled with field spectra (as shown in Kiriburu as well as Meghahatuburu mining and surrounding forest areas) than any other multispectral data (Landsat).

In the VIs model 1 based forest health study, maximum correlation coefficients and separability values were obtained from the MNDVI705. The MNDVI705 index works well with the lower chlorophyll content, so it is accepted for appreciable forest health results (Kumar et al., 2015). The test of forest health results for leaf pigment's VIs is relatively lower than any other vegetation indices. In leaf pigment VIs, the value of ARI1 is high than other VIs (Penuelas et al., 1994). For light use efficiency, VIs value

is relatively higher than that of leaf pigment VIs (Jenkins et al., 2007). NDNI is a useful index where there exhibits a high variability in the canopy or leaf pigment structure (Rodríguez et al., 2007). The test result for the canopy water content index was low because of vegetation canopy structure (Sims et al., 2002). In general, VIs correlation and separability values were compared with the earlier forest health studies (Tuominen et al., 2009) have shown the highest correlation and separability values with NDVI (broad-bands); MNDVI705 (Narrow-bands) for greenness VIs, ARI1 (Narrow-bands) for leaf pigment VIs and MSI (Narrow-bands) for canopy water content VIs.

The reflectance spectra for the healthy forest were recorded higher in the near-infrared region. The reflectance spectra for the unhealthy forest were recorded lower in the near-infrared region. The near-infrared (NIR) region shows higher value due to high chlorophyll pigment spectra, and the leaf's chlorophyll pigment spectra are closest to the canopy (Carter et al., 2001). The result was matched with the previous study about the tree's leaf reflectance spectra and had shown a positive correlation (Curran, 1989; Curran and Peterson, 2001). Although the two reflectance spectra for different forest health status are sufficiently analogous, yet the amplitude of lab reflectance spectra is always higher than Hyperion image reflectance spectra. The Hyperion image reflectance spectra has a lower amplitude as it has a weak signal-to-noise ratio.

Landsat-OLI image classification by SVM algorithm, showing the overall accuracy of 67.21% and a kappa statistic of 0.62. Hyperion image-based classification (VIs model) got an overall accuracy of 81.52 % and a kappa statistic of 0.79. The forest health classification educed by the VIs model classifier on Hyperion image showed better results than SVM algorithm classification on Landsat-OLI image. The forest health classification by SAM algorithm (Overall accuracy: 79.55%, kappa statistics: 0.75) shown the better result than SVM algorithm-based classification (76.53%, kappa statistics: 0.71) on Hyperion image. Hyperion image-based VIs model (Overall Accuracy: 81.52%, Kappa Statistics: 0.79) for forest health classification shown the best result among all the classifications. Some previous studies have shown the undertaking for getting better forest health classification through Hyperspectral remote sensing. George et al., (2014) shown the better forest classification through Hyperspectral remote sensing and compared the classification results obtained from Hyperion and Landsat TM sensors for the study of Western Himalaya and obtained

collective accuracies of 81.52 % and 69.62 % respectively. Thenkabail et al., 2004 compared the classification results of different sensors viz., Hyperion, IKONOS, ALI, and ETM+ sensors for the study of African rainforests and obtained collective accuracies of 93.2%, 87.46 %, 81.53%, and 76.9% respectively.

The forest health risk arises from mining dust, which may lead to the plant's growth problem (Tuominen et al., 2009). A good correlation was observed between the distance from (Kiriburu and Meghahataburu) mines, foliar dust concentration, and forest health classes. This relationship indicates that the quality of the forest depends on the distance from mines and foliar dust concentration as well. Tuominen et al. (2008) showed a clear relationship between leaf reflectance and tree's distance from mines. The result obtained for both the mining areas (Kiriburu and Meghahatuburu) has a strong correlation. This reason being the same type of vegetation, foliar dust concentration and distance from mines.

This work involved, the validation (R^2) of forest health result as well as standard error (S) and shown on a scatter-matrix error plot. There may be various reasons behind the error in the forest health result. Hyperion satellite image spectra have a lower amplitude as it has a higher noise ratio (Shaw et al., 2003). Hyperion satellite image spectra also get affected by atmospheric components. Infield spectra, during the time of data collection, some noise data were also self-generated (Vaiphasa, 2006). The field Spectroradiometer has different inherent variation in detector sensitivity with the varying temperature causes temperature drifts error. The study area is located in the hilly region, which induces the shadow effect on the satellite image (Ittenn & Meyer, 1993). The spatial resolution of the Hyperion image is 30 × 30 meter pixel, which consequences to the problem of mixed pixels in the study area (Lee & Lathrop, 2005).

4.5 Summary

This chapter aimed at describing the potential of Hyperion and Landsat satellite imagery, ground tree spectra data and foliar dust data for forest health assessment in Kiriburu and Meghahataburu iron ore mines and its vicinage. This work is first of its kind, which attempts to use hyperspectral satellite data with field spectra data to assess forest health and correlate it with mines induced foliar dust and environment. The study focuses on the particular section of 21 wave-bands from hyperspectral remote sensing data, and classification is done on the VIs tool, SVM, and SAM algorithms for

yielding better forest health assessment results. In this study, a good correlation was shown between forest health and distance from mines with leaf dust. It means that as the mining area increases forest as well as the environment will also get affected. We hope that our work could serve as the base, and the methodology can also be applied to different mines related forest areas with certain modifications in the forest health parameters. The forest health map obtained provides a guideline for geo-environmental planning and management in mining proximity forest area.